AGU PUBLICATIONS

JGR

Journal of Geophysical Research: Oceans

RESEARCH ARTICLE

10.1002/2017JC012890

Key Points:
- Distribution pattern and mass budget of polycyclic aromatic hydrocarbons in the Eastern China Marginal Seas was depicted
- Hydrodynamics, sediment properties, and anthropogenic impacts influence the distribution of polycyclic aromatic hydrocarbons
- River discharges and atmospheric deposition constitute 28.4% and 71.6% of total input, respectively; 88.4% of PAHs influx is buried

Supporting Information:
- Supporting Information S1

Correspondence to:
X. Zou,
zouxq@nju.edu.cn

Citation:
Wang, C. L., X. Q. Zou, Y. F. Zhao, Y. L. Li, Q. C. Song, T. Wang, and W. W. Yu (2017), Distribution pattern and mass budget of sedimentary polycyclic aromatic hydrocarbons in shelf areas of the Eastern China Marginal Seas, *J. Geophys. Res. Oceans*, *122*, 4990–5004, doi:10.1002/2017JC012890.

Received 14 MAR 2017
Accepted 28 MAY 2017
Accepted article online 6 JUN 2017
Published online 21 JUN 2017

© 2017. American Geophysical Union. All Rights Reserved.

Distribution pattern and mass budget of sedimentary polycyclic aromatic hydrocarbons in shelf areas of the Eastern China Marginal Seas

C. L. Wang[1,2], X. Q. Zou[1,2], Y. F. Zhao[1,2], Y. L. Li[1,2], Q. C. Song[1,2], T. Wang[1,2], and W. W. Yu[1,2,3]

[1]Key Laboratory of Coast and Island Development (Nanjing University), Ministry of Education, Nanjing, China, [2]School of Geographic and Oceanographic Sciences, Nanjing University, Nanjing, China, [3]Marine Fisheries Research Institute of Jiangsu Province, Nantong, China

Abstract This study conducted the first extensive and comprehensive investigation of the regional-scale sedimentary polycyclic aromatic hydrocarbons (PAHs) concentration, flux, and budget in the continental shelves of the Eastern China Marginal Seas (ECMSs). Surface sediment samples from multiple sites were collected and assessed, and the latest data from current research were assessed. The spatial distribution pattern of PAHs in the ECMSs was significantly influenced by the regional hydrodynamics, sediment properties (grain-size, total organic carbon [TOC] content, and sedimentation rate), and anthropogenic impacts. Relatively higher PAHs concentrations occurred in areas with fine-grained sediment. Results of source apportionment found that the relative proportions of PAHs showed significant regional variation, mainly influenced by socioeconomic differences between north and south China. The PAHs burial flux in the study area ranged from 11.2 to 1308 ng cm^{-2} yr^{-1} with an average value of 101 ± 104 ng cm^{-2} yr^{-1}. The area-integrated sedimentary PAHs burial flux across the ECMSs was 494 t yr^{-1}. A mass budget calculation revealed that riverine input and atmospheric deposition were the most significant sources contributing, 28.4% and 71.6%, respectively. The study demonstrated that net PAHs transportation occurs between the Bohai Sea (BS) and Yellow Sea (YS), with a flux of approximately 10.2 t yr^{-1}. PAHs were also transported from YS to the East China Sea (ECS), due to water exchange between the YS and ECS. Additionally, substantial amounts of PAHs in the inner shelf of the ECS were transported out of the shelf area due to cross-shelf plume.

1. Introduction

Coastal and shelf regions are important oceanic realms in terms of human activity and biological diversity, and are among the most sensitive and vulnerable areas on earth [*Bouloubassi et al.*, 2012]. The influence of anthropogenic activities and biogeochemical processes in coastal zones is critical to ecosystem preservation [*Lipiatou et al.*, 1997; *Bianchi*, 2011]. Therefore, researchers are focusing on regional and global oceanic carbon and nitrogen cycles, fate of environmental pollutants, and transportation of nutrients in coastal ocean ecosystems [*Fang et al.*, 2015; *Lin et al.*, 2016; *Bouloubassi et al.*, 2012]. Increasing human activities have threatened services and goods provided by coastal marine ecosystems, due to increases in surface runoff, riverine discharge, and industrial and domestic wastewater discharges. Consequently, coastal oceans are recognized as important sinks of various materials such as organic carbon, heavy metals, nutrients, and persistent organic pollutants (POPs), among others [*Leithold et al.*, 2016; *Gao et al.*, 2014; *Xing et al.*, 2017; *Mwangi et al.*, 2016]. In recent years, the focus on POPs, especially polycyclic aromatic hydrocarbons (PAHs), in coastal marine ecosystems has increased, due to their adverse effects on marine organisms.

PAHs mainly originate from anthropogenic activities such as vehicle emissions and incomplete combustion of fossil fuels and biomass [*Sverdrup et al.*, 2002; *Han et al.*, 2015]. They are known for their toxic, carcinogenic, mutagenic, bio-accumulative, and persistent characteristics [*Liu et al.*, 2012a; *Khairy et al.*, 2014]. The U.S. Environmental Protection Agency has identified 16 PAHs as priority pollutants. Anthropogenic PAHs are omnipresent in environmental matrices and are found in the atmosphere, soil, water, ice, sediment, and food web [*Chen et al.*, 2016; *C. Wang et al.*, 2015; *Lohmann et al.*, 2009; *Yuan et al.*, 2014; *Stout and Graan*, 2010; *Huang and Batterman*, 2014], due to the global distribution of sources and the resistance of PAHs to

degradation. Marine sediments usually act as important sinks for anthropogenic PAHs through two major pathways, riverine discharge and atmospheric deposition [*Wang et al*., 2007; *Mulder et al*., 2014; *González-Gaya et al*., 2016]. Following release into the marine environment, most PAHs bind to fine particles, due to their high hydrophobicity and lipid solubility, and are deposited in the bottom sediments. [*Kim et al*., 1999; *Li et al*., 2006]. More than 90% of global riverine sediments are buried on the continental shelf, though the continental shelf accounts for only 10% of the area of the global ocean [*Deng et al*., 2006]. Consequently, the sedimentary PAHs buried in the continental shelf play a key role in the global PAHs cycle, by linking the terrestrial, oceanic, and atmospheric PAHs reservoirs. Moreover, PAHs contain large amounts of carbon, and previous studies have demonstrated that semivolatile organic compounds, including PAHs, have significant roles in the carbon cycle [*Park et al*., 2013; *González-Gaya et al*., 2016]. Global atmospheric PAHs input to the global ocean is about 1.08 Tg yr^{-1}, and these PAHs are a significant component of global carbon deposition, estimated at 400 Tg yr^{-1} of carbon, or approximately 15% of the oceanic CO_2 uptake [*González-Gaya et al*., 2016]. Therefore, in addition to posing a threat to marine organisms, PAHs play an important role in oceanic carbon biogeochemical cycles. PAHs emissions from Asia contributed approximately 55% of the global atmospheric PAHs emissions, and the highest emitter was China [*Zhang and Tao*, 2009]. The continental shelves of the Eastern China Marginal Seas (ECMSs, including Bohai Sea [BS], Yellow Sea [YS], and East China Sea [ECS]) constitute a part of the Asian continental outflow pathway to the western Pacific Ocean, driven by the East Asian monsoon [*Lang et al*., 2008; *Li et al*., 2016]. Approximately 4664 t of PAHs are transported to the BS, YS, and ECS annually.

The ECMSs are gigantic marginal sea systems in the western Pacific Ocean and one of the largest convergence regions between the world's largest continent (Asia-Europe) and the Pacific Ocean. Moreover, the Changjiang (Yangtze) River and Huanghe (Yellow) River have discharged approximately 480×10^6 and 1000×10^6 t of sediment, respectively, to the ECMSs throughout history [*Xu et al*., 2012], or approximately 10% of the global sediment discharge. The ECMSs are adjacent to one of the world's most heavily populated and densely developed regions (Changjiang [Yangtze] River basin with 400 million inhabitants) [*Zhao et al*., 2015], and receive large amounts of terrestrial pollutants [*Lin et al*., 2013; *Zhong et al*., 2014; *Li et al*., 2017]. In the early 21st century, several ECMSs-related studies focused on the PAHs cycle, important factors that regulate PAHs budgets, fate of PAHs in the marine environment [*Liu et al*., 2006; *Lin et al*., 2011; *Li et al*., 2012], deposition flux of sedimentary PAHs [*Guo et al*., 2006; *Qin et al*., 2011; *Lin et al*., 2013], and air-seawater exchange of PAHs [*Wang et al*., 2013; *Chen et al*., 2016]. However, PAHs research efforts have concentrated on specific compartments and regions due to the complexity and size of the ECMSs region. Limited attention has been paid to the distribution patterns and mass budget of PAHs in the ECMSs region as a whole, although this would be essential to understanding the significance of ECMSs on the regional and global PAHs cycles.

The present study explores the distribution patterns of PAHs and factors that influence PAHs levels in the ECMSs. Regional hydrodynamics, grain-size distribution, total organic carbon (TOC) content, sedimentation rate, and depositional flux were analyzed in the context of the regional socioeconomic structure and anthropogenic impacts. This study also attempts to construct a preliminary mass budget for sedimentary PAHs in the ECMSs based on the most recent data in the published literature. To the best of our knowledge, this is the first study to estimate the mass budget of sedimentary PAHs on an extensive regional scale.

2. Materials and Methods

2.1. Regional Settings

The BS is a shallow enclosed sea with an area of 77,000 km^2, mean depth of approximately 18 m, and mean tidal current varying from 0.2 to 0.8 m/s [*Huang et al*., 1999]. The circulation pattern in the BS consists of an inflow via the northern section of the Bohai Strait and an outflow via the southern section [*Zeng et al*., 2015; *Bian et al*., 2013]. The YS is a semiclosed shallow sea with area of 400,000 km^2, and mean depth of approximately 44 m. Circulation patterns in the YS exhibit distinct seasonal variation. In winter, the strong Yellow Sea Warm Current (YSWC) flows northward through the middle of the YS, while the relatively weak Yellow Sea Coastal Current (YSCC) flows southward. In summer, the YSCC flows north but the YSWC is so weak that it only reaches the area north of Cheju Island [*Xia et al*., 2006; *Zeng et al*., 2015]. The ECS is a relatively open marginal sea linked with the Pacific Ocean, with an area of 770,000 km^2 and shelf area of approximately

21699291, 2017, 6, Downloaded from https://agupubs.onlinelibrary.wiley.com/doi/10.1002/2017JC012890 by Nanjing University, Wiley Online Library on [07/06/2024]. See the Terms and Conditions (https://onlinelibrary.wiley.com/terms-and-conditions) on Wiley Online Library for rules of use; OA articles are governed by the applicable Creative Commons License

550,000 km^2. The mean depth of the ECS is approximately 77 m [*Dong et al.*, 2011]. The circulation of the ECS exhibits seasonal variation and mainly consists of the Zhejiang–Fujian Coastal Current (ZFCC), controlled by the East Asian monsoon, and the Taiwan Warm Current (TWWC) [*Zhang et al.*, 2015; *Zhao et al.*, 2017]. In winter, the ZFCC is strong and flows southward due to the prevailing winter monsoon, but the flow direction of the ZFCC becomes northward in summer due to southerly winds [*Yuan and Hsueh*, 2010].

The coastal and upland zones of the ECMSs span six coastal provinces (Liaoning, Hebei, Shangdong, Jiangsu, Zhejiang, and Fujian), five inland provinces (Inner Mongolia, Shanxi, Henan, Anhui, and Jiangxi), and three municipalities under the direct jurisdiction of the Central Government in China (Beijing, Tianjin, and Shanghai). The area near the ECMSs is the most densely populated and economically and industrially developed region in China. These provinces and mega-cities host more than half the national population, contribute almost 60% of the national GDP, and were responsible for 60.7% of national coal consumption in 2014 (http://www.stats.gov.cn/english). Therefore, large amounts of terrestrial and atmospheric contamination, including PAHs, were discharged into the ECMSs.

2.2. Experimental Section

2.2.1. Sample Collection, Preparation, and Cleanup

In 2013, 77 surface sediment samples (0–2 cm depth) were collected from the estuarine-inner shelf of the ECS using a stainless-steel grab sampler. All samples were placed into precleaned (baked and solvent-rinsed) aluminum foil and stored at −20°C prior to analysis.

Detailed information about PAHs extraction and analysis is described in our previous study [*C. Wang et al.*, 2016b], and a brief outline is provided here. Surface sediments were freeze dried, and then gently ground and sieved. 5 g of the dried sediment sample, together with 2 g of activated copper, underwent Soxhlet extraction in 100 mL acetone/n-hexane (1:1 v/v) for 24 h. A three-step cleanup was then used to purify the extracted solution. The extract was first concentrated to a volume of 1–2 mL using a rotary evaporator; the concentrated solution was then applied to a 10 mm id chromatography column containing 5 g of silica gel

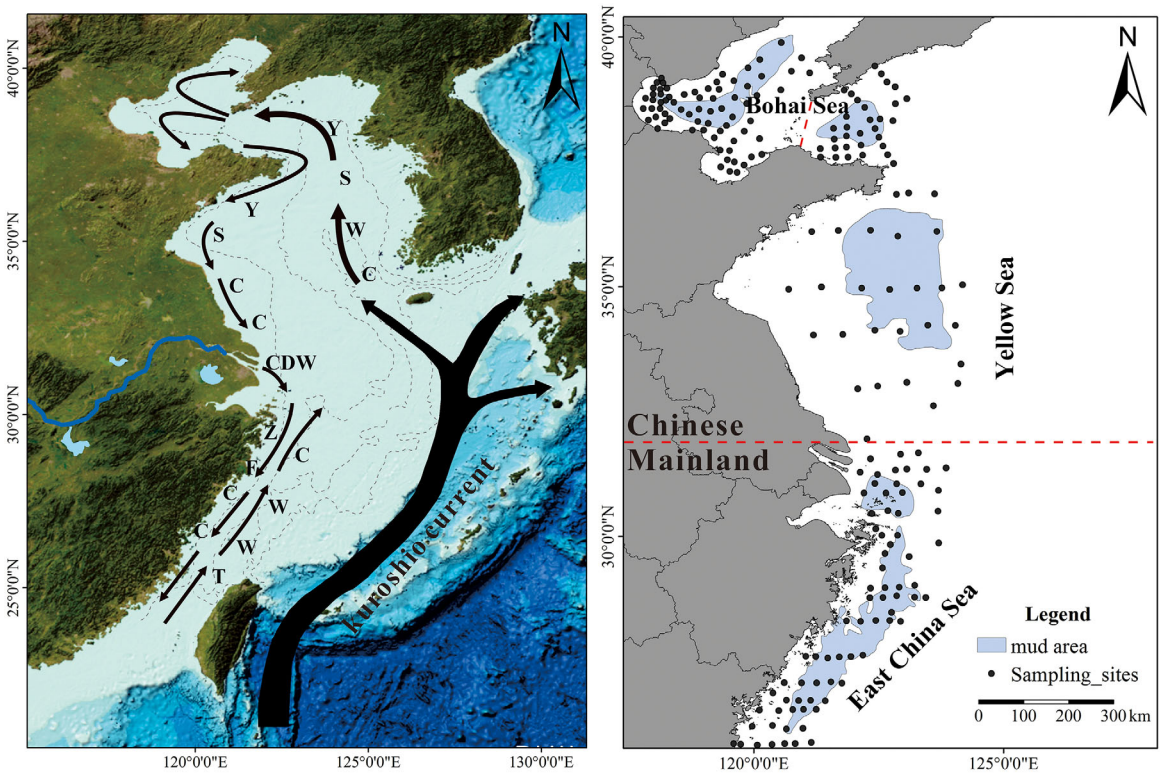

Figure 1. Location (a) map and (b) sampling sites located in the ECMSs. TWWC, Taiwan Warm Current; ZFCC, Zhejiang-Fujian Coastal Current; YSCC, Yellow Sea Coastal Current; YSWC, Yellow Sea Warm Current; CDW, Changjiang Diluted Water.

21699291, 2017, 6, Downloaded from https://agupubs.onlinelibrary.wiley.com/doi/10.1002/2017JC012890 by Nanjing University, Wiley Online Library on [07/06/2024]. See the Terms and Conditions (https://onlinelibrary.wiley.com/terms-and-conditions) on Wiley Online Library for rules of use; OA articles are governed by the applicable Creative Commons License

and 2 cm anhydrous sodium sulfate and eluted with 50 mL dichloromethane/n-hexane (3:2 v/v). Finally, the eluent was vacuum-evaporated and exchanged with n-hexane, and concentrated to 1 mL.

2.2.2. Chemical Analysis

Specific analytes included 16 priority PAHs: naphthane (Nap), acenaphthylene (Acy), acenaphthene (Ace), fluorene (Flu), anthracene (Ant), phenanthrene (Phe), benzo[a]anthracene (BaA), chrysene (Chr), fluoranthene (Flo), pyrene (Pyr), benzo[a]pyrene (BaP), dibenzo[a,h]anthracene (DahA), benzo[b]fluoracene (BbF), benzo[k]fluoracene (BkF), benzo[g,h,i]perylene (BghiP), and indeno[1,2,3-cd]pyrene (IcdP). All PAHs standards were purchased from Supelco (Bellefonte, PA, USA).

The samples were analyzed on a Shimadzu QP2010 Ultra GC-MS, fitted with a fused silica capillary Rtx-5MS column (30 m $\times$ 0.25 mm internal diameter, 0.25 μm film thickness). The carrier gas was helium, with a flow rate of 1.0 mL min^{-1}. The GC temperature procedure was as follows: initial temperature of 80°C (held for 2 min), increased to 180°C at a rate of 20°C min^{-1} and held for 5 min, then increased to 290°C at a rate of 10°C min^{-1} and held for 15 min. The ionization was carried out in the electron-impact mode at 70 eV, and all samples were analyzed in the selective-ion monitoring mode.

2.2.3. Quality Assurance/Control

Glassware and sodium sulfate were baked for 5 h at 450°C, and glassware was subsequently rinsed three times with n-hexane, dichloromethane, and acetone before use. All solvents used were HPLC grade (Tedia CO. Inc., USA). Silica gel (200 mesh, Qingdao Haiyang Chemical CO. Inc., Shandong, China) was extracted using n-hexane, dichloromethane, and acetone, and activated at 130°C for 16 h.

A procedural blank containing only copper was subjected to the same cleanup and concentration steps, and analyzed alongside the sediment samples with every six-sample set. Matrix-spiked samples (sediments pre-extracted and baked for 5 h at 450°C to remove PAHs and then spiked with PAHs standards) were also analyzed with every six-sample set, to determine percentage of recovery, which has been demonstrated to be effective by *Wang et al.* [2015]. The average recoveries of 16 PAHs based on the matrix-spiked samples ranged from 74.5% to 106.2%. An external standard method was used to quantify the concentration of 16 PAHs in this study.

2.3. Data Collection

Data values for PAHs concentration (n = 204) (Figure 1b), sedimentation rates (n = 202), and TOC content (TOC, n = 386) in sediment samples were collected, consolidated, and processed further using the Kriging interpolation method. PAHs concentration data were mainly obtained from *Qin et al.* [2011], and *Lin et al.* [2011, 2013] and TOC contents were derived from *Qin et al.* [2011], *Hu et al.* [2012], *Lin et al.* [2013], *Zeng et al.* [2012], and *Xing et al.* [2014]. Sedimentation rates were mainly obtained from *Hu et al.* [2011], *C. Wang et al.* [2016b], and references therein. The original data set on sediment grain-size was mainly found in *Hu et al.* [2009, 2013] and *Lin et al.* [2013].

Deposition flux of PAHs in the surface sediments was estimated to assess the extent of contamination and the potential toxicity. The deposition flux was calculated using several sediment properties and measured PAHs concentrations, as shown in equation (1).

$$F_{deposition} = 10^{10} \cdot A \cdot C_{PAHs} \cdot \rho \cdot \omega \cdot (1-\varphi) \quad (1)$$

where, A is the area of a given region (km^2), C_{PAHs} is the measured sedimentary PAHs concentration (ng g^{-1}), ρ is the dry density of the sediment samples (g cm^{-3}), ω is the sedimentation rate (cm yr^{-1}), and φ is the sediment porosity (dimensionless). Porosity is widely measured in sediment mixing layers around the world and ranges from 0.7 to 0.8 [*Ali et al.*, 2014; *Fang et al.*, 2015]. We selected a median value of 0.75 to represent sediment porosity in the study area. A recommended value of 1.2 g cm^{-3} was selected for ρ [*Liu et al.*, 2007]. The Kriging interpolation method was used to obtain the spatial distribution of ω, based on accurately dated values collected in the study area.

3. Results and Discussion

3.1. Background Depositional Setting: Distribution Patterns of Grain-Size and TOC

3.1.1. Distribution Patterns of Grain-Size and Sedimentation Rate in the ECMSs

The general distribution pattern of grain-size in the ECMSs determined by this study was consistent with findings of previous studies [*Hu et al.*, 2016a; *Lin et al.*, 2013], which reported several mud deposits

21699291, 2017, 6, Downloaded from https://agupubs.onlinelibrary.wiley.com/doi/10.1002/2017JC012890 by Nanjing University, Wiley Online Library on [07/06/2024]. See the Terms and Conditions (https://onlinelibrary.wiley.com/terms-and-conditions) on Wiley Online Library for rules of use; OA articles are governed by the applicable Creative Commons License

composed primarily of silt and clay (with a finer median grain, Md 6–7 Φ), in Bohai Bay (BB), the central YS, the Changjiang Subaqueous Delta (SCD), and the ECS inner shelf (Figure 2a). Sediments in the semienclosed BB mainly originated from the Luanhe (2.67×10^7 t yr^{-1}) and Haihe (6×10^6 t yr^{-1}) Rivers [*Qin et al.*, 1990], and grain-size ranged from 5.37 to 7.55 Φ, with an average value of 6.6 Φ. Mud deposits in the central YS (grain-size from 3.24 to 7.70 Φ, with an average value of 5.21 Φ) were not directly sourced from rivers. Other large mud deposits are located at the estuarine–inner shelf region of the ECS, which comprises two subregions, the SCD mud area (SCDMA) and Zhejiang-Fujian coastal mud area (ZFCMA) [*Liu et al.*, 2007]. These mud deposits (grain-size from 1.91 to 8.65 Φ, with an average value of 5.85 Φ) are mainly controlled by Changjiang-derived sediments and regional marine dynamics. Overall, the distribution pattern of grain-size in the ECMSs mainly reflected river input and regional marine dynamics.

As seen in Figure 2b, the distribution of sedimentation rates in the ECMSs presents a significant difference. The sediment accumulation rate, on a time scale of 100 years, was extremely high near the Huanghe (Yellow) River Estuary (HRE), as large amounts of sediment discharged from the Huanghe (Yellow) River are trapped and deposited in this area. Compared to the HRE, sediment accumulation rates in the BB, open BS, and YS were relatively slow as these areas lack large river discharges. The BB received sediment from the Haihe and Luanhe Rivers, leading to higher sedimentation rates than found in the open BS and YS. The open BS and YS received small portions of Huanghe-derived sediments, transported by regional hydrodynamics. Atmospheric deposition also serves as a sediment source in the BS and YS, as they are downwind of the Asian continental outflow during spring and winter [*Lin et al.*, 2011]. Under the influence of the East Asian monsoon, considerable amounts of aeolian dust from northwest China and Mongolia are transported and deposited into the marginal seas [*Zhang and Gao*, 2007]. The region with second highest sedimentation rate is located in the CSD, and is influenced by the Changjiang (Yangtze) River. The sedimentation rate in the ZFCMA is also relatively high (Figure 2b), due to Changjiang-derived sediments.

3.1.2. Distribution Pattern of Sedimentary TOC in the ECMSs

TOC content over the study area varied over a relatively broad range from 0.08% to 1.37%, with a mean value of 0.37% (Figure 3b). The distribution pattern of TOC was fairly similar to of sediment grain-size (Figure 2a)

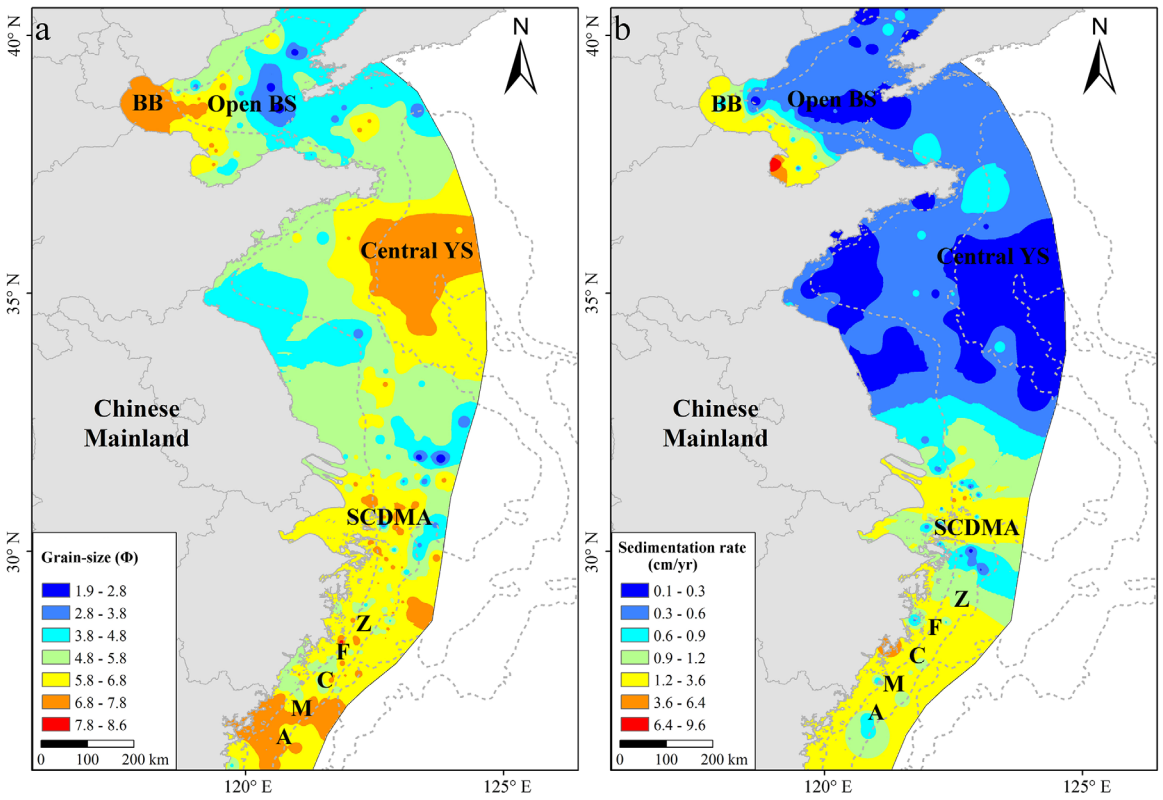

Figure 2. The distribution patterns of sediment grain-size and sedimentation rate of the ECMSs.

21699291, 2017, 6, Downloaded from https://agupubs.onlinelibrary.wiley.com/doi/10.1002/2017JC012890 by Nanjing University, Wiley Online Library on [07/06/2024]. See the Terms and Conditions (https://onlinelibrary.wiley.com/terms-and-conditions) on Wiley Online Library for rules of use; OA articles are governed by the applicable Creative Commons License

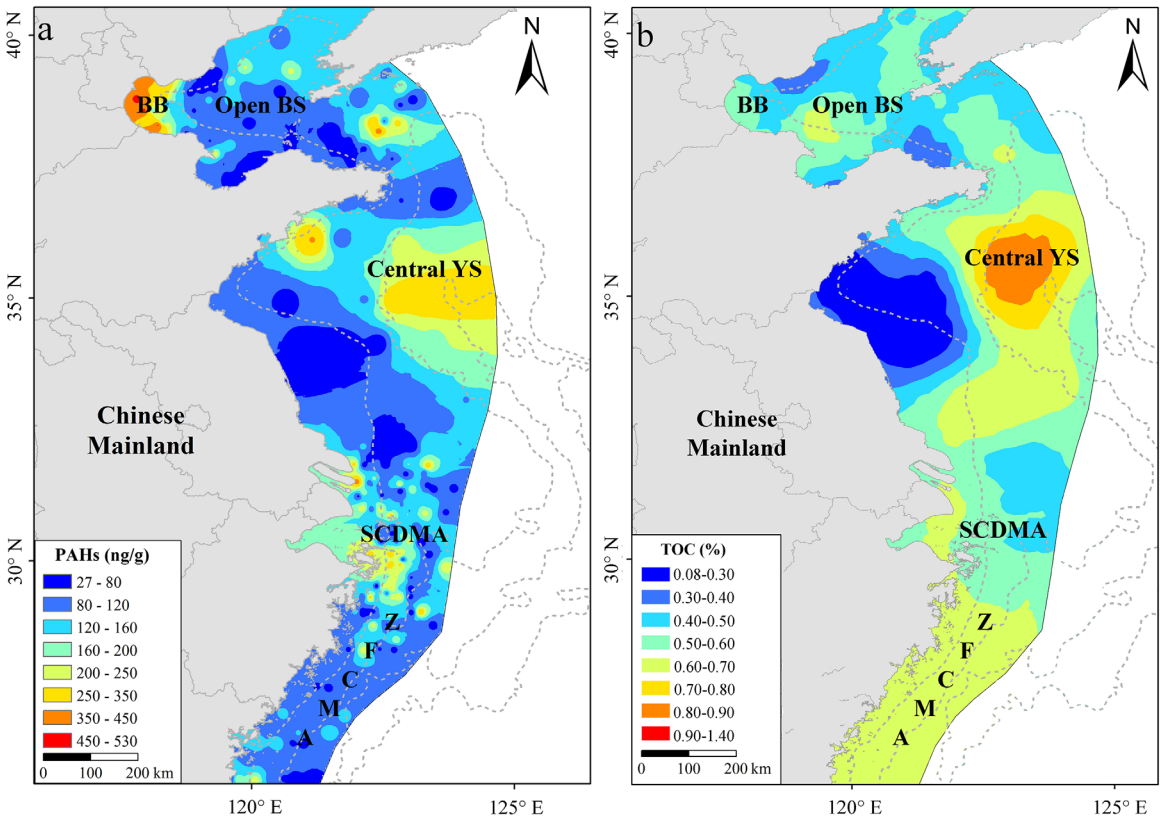

Figure 3. The distribution patterns of PAHs and TOC in the ECMSs.

(correlation coefficient $>$ 0.5), indicating relatively high TOC content in the central YS, SCDMA, and ZFCMA (Figure 3b). Low TOC content ($<$0.3%) mostly occurred in the Bohai Strait and western YS, which were probably influenced by strong hydrodynamics, relatively coarser sediment grain-size, and low sedimentation rates. Bohai Strait is the water exchange channel between the BS and YS, with high flow velocity only relatively coarser particles are retained. Sediments in the western YS were mainly composed of coarse particles (fine sand, sandy silt, and silty sand), which mainly originated from coastal erosion in the old HRE. The highest TOC content was observed in the central YS, which is subject to cyclonic circulation leading to substantial deposition of fine particles in the area (Figure 2a). Moreover, relatively high content of TOC occurred in the SCDMA and ZFCMA (Figure 3b) as large amounts of TOC were discharged along with Changjiang-derived sediments.

3.2. Distribution Patterns of PAHs and Their Constraining Factors

3.2.1. Distribution Patterns of PAHs in the ECMSs

Total concentration of the 16 PAHs (ΣPAHs) over the entire sampling area showed a relatively broad range, varying between 26.38 and 537.60 ng g^{-1}, with an average value of 231.21 ng g^{-1} (Figure 3a). Relatively high ΣPAHs concentrations were observed in the BB, central YS, and SCDMA, and the distribution was generally consistent with that of sediment grain-size. The ΣPAHs in the BB (324–446 ng g^{-1}, with a mean value of 400 ng g^{-1}) was relatively higher than that in the YS and SCDMA. BB is surrounded by industrial cities such as Tanshan and Tianjin, and is an important component of the Bohai Economic Rim. BB is also an important oil-producing region, surrounded by busy oilfields such as Dagang and Shengli. Therefore, large amounts of surface runoff containing domestic sewage, industrial effluent, and mining wastewater are discharged into the BB. *Bai and Sun* [2007] illustrated that water exchange in the BB is relatively slow, resulting in inefficient diffusion of pollutants in this region. In addition, Figure 2a shows that surface sediments in the BB are dominated by fine particles that easily absorb PAHs. Thus, multiple factors, including anthropogenic activities, hydrodynamics, and sedimentary features, have contributed to relatively high ΣPAHs in the BB. The ΣPAHs levels in the central YS and SCDMA are also high (Figure 3a), again consistent with the distribution patterns of sediment grain-size and TOC contents. The ΣPAHs levels in the central YS are mainly controlled by

21699291, 2017, 6, Downloaded from https://agupubs.onlinelibrary.wiley.com/doi/10.1002/2017JC012890 by Nanjing University, Wiley Online Library on [07/06/2024]. See the Terms and Conditions (https://onlinelibrary.wiley.com/terms-and-conditions) on Wiley Online Library for rules of use; OA articles are governed by the applicable Creative Commons License

Table 1. Correlation Coefficient Matrix of PAHs and Sediment Features in the ECMSs

	High-Weight PAHs	Low-Weight PAHs	ΣPAHs	Grain-Size	TOC
High-weight PAHs	1.000				
Low-weight PAHs	0.403	1.000			
ΣPAHs	0.807	0.866	1.000		
Grain-size	0.372	0.497	0.524	1.000	
TOC	0.348	0.179	0.306	0.568	1.000

sedimentary features and hydrodynamics. Previous studies have demonstrated that sediments in the central YS mainly originated from the Huanghe (Yellow) River, under the influence of the YSCC and YSWC [*Yang and Liu*, 2007; *Hu et al*., 2016a]. Huanghe-derived sediments discharged into the BS were transported along the Shandong Peninsula by coastal currents and trapped by cyclonic circulation in the central YS. Therefore, PAHs associated with river-derived sediments were also trapped and deposited, resulting in relatively high ΣPAHs. Unlike the central YS, PAHs in the ECS were directly influenced by river input. Changjiang-derived sediments discharged into the ECS were deposited in the estuary to form the SCDMA, consequently transporting substantial sedimentary PAHs in this region. The range of ΣPAH in the SCDMA is 239–324 ng g^{-1}, with an average of 330 ng g^{-1} (Figure 3a). During winter, sediments trapped in the SCDMA are resuspended due to the strong winter monsoon, and transported southward along the Zhejiang-Fujian Coast. Therefore, significant amounts of PAHs were transported southward and deposited along the coast. Overall, the distribution patterns of PAHs in the ECMSs were mainly controlled by the combination of river inputs, hydrodynamics, and sedimentary features.

Some studies have confirmed correlation between PAHs concentrations and both sediment grain-size and TOC concentration [*Li et al*., 2006; *Hu et al*., 2014], while others have questioned the correlation [*C. Wang et al*., 2016b; *Lin et al*., 2013; *Yim et al*., 2014]. In order to assess the correlation between PAHs concentrations with sediment grain-size and TOC content, our study examined the correlations individually. Considering the otherness of the sampling sites in different indexes, an assimilation method was used in this study. First, all indexes were interpolated based on the existing sampling sites to obtain spatial distribution patterns. Second, the "Fishnet" technology in ArcGIS 10.2 was used to acquire a series of new virtual sampling sites with unified position coordinates in our study area. Third, the "Extract values to points" operation in ArcGIS 10.2 was used to acquire attribute values for each new virtual sampling site. At this point, the process of data assimilation was complete, and we had obtained a data set with PAHs concentration, sediment grain-size, and TOC concentration. Correlation analyses indicated that significant correlations existed between PAHs concentrations and sediment grain-size on this extensive regional scale, but not between PAHs concentrations and TOC contents (Table 1). This probably reflects regional differentiation of sediment sources, regional hydrodynamics, TOC sources, and others. The ECMS is a large and complex system, with different depositional processes, hydrodynamics, and material sources. These results suggest that PAHs concentrations in the sediment are not controlled by any single factor, but depend on multiple factors [*C. Wang et al*., 2016b].

3.2.2. Anthropogenic Impacts

Previous studies have demonstrated that environmental changes caused by anthropogenic activities are recorded in marine sediment as chemical residues are buried by depositional processes [*Lima et al*., 2003; *Guo et al*., 2006; *Liu et al*., 2013]. *Liu et al*. [2012b] reconstructed the evolution of anthropogenic activities in mainland China by characterizing PAHs in sediment cores from the YS and South China Sea. Some researchers have discussed the sources and compositions of PAHs in the ECMSs at different scales and in different regions [*Qin et al*., 2011; *Lin et al*., 2011, 2013; *C. Wang et al*., 2016b]. However, these studies focused on local dynamics, and an integrated study on the ECMSs is lacking. For the present study, we collected the results of source apportionment of PAHs from published materials [*Lin et al*., 2011, 2013; *C. Wang et al*., 2016b] to understand the distribution patterns of PAHs with different sources in different regions of the ECMSs. All of these results are acquired by a positive matrix factorization model, demonstrated to be effective by *Shi et al*. [2009] and *Zhang et al*. [2012]. We also attempted to include the socioeconomic structure of the coastal provinces and current systems in the ECMSs to explore factors controlling the distribution patterns of PAHs in these regions. The ECMSs were divided into six subregions (BB, BS, North YS (NYS), South YS (SYS), SCDMA, and ZFCMA), based on the compositions of PAHs, physicochemical properties of sediments, and regional hydrodynamics. Three main PAHs sources, petrogenic sources, coal combustion, and vehicle emissions, were selected to identify different distribution patterns of PAHs in the subregions of the ECMSs, as shown in Figure 4.

21699291, 2017, 6, Downloaded from https://agupubs.onlinelibrary.wiley.com/doi/10.1002/2017JC012890 by Nanjing University, Wiley Online Library on [07/06/2024]. See the Terms and Conditions (https://onlinelibrary.wiley.com/terms-and-conditions) on Wiley Online Library for rules of use; OA articles are governed by the applicable Creative Commons License

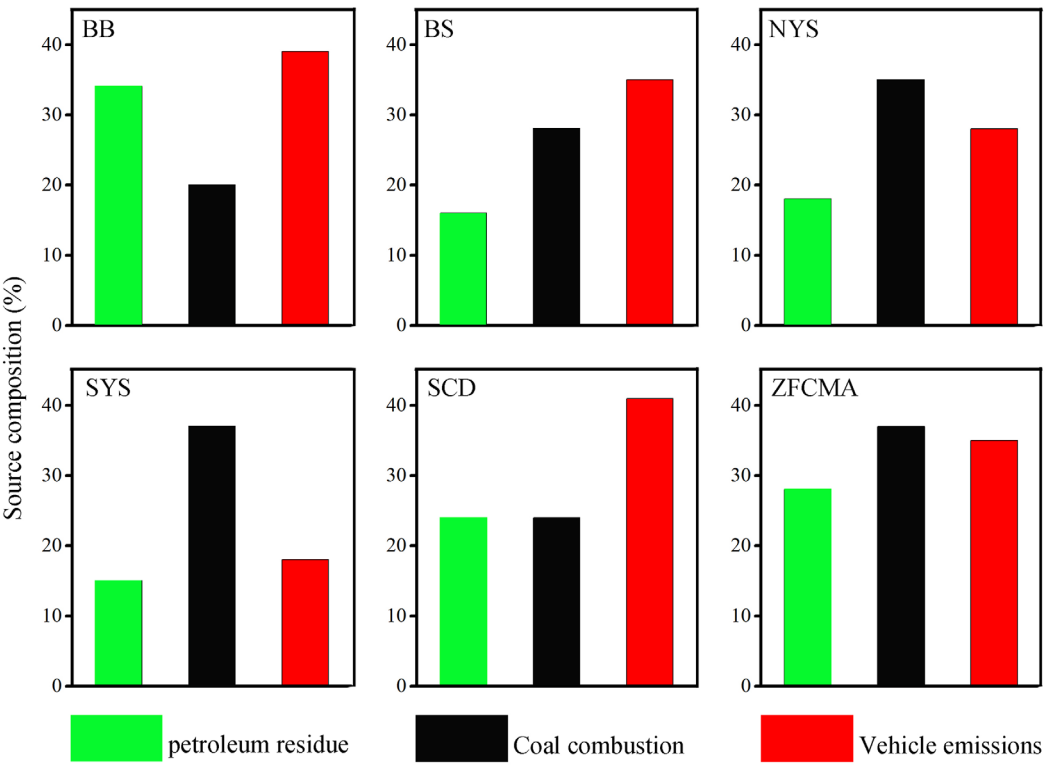

Figure 4. Source compositions and contributions of PAHs in the ECMSs.

Figure 4 highlights that the different composition and sources of PAHs in different subregions in the ECMSs. Firstly, PAHs originating from coal combustion were mainly found in the north part of the ECMSs such as BS and YS. The proportion of PAHs from coal combustion showed an increasing trend from the BB (19%) to SYS (37%) (Figure 4). *Liu et al.* [2012b] reported that variable lifestyles and economic development are important factors influencing the distribution of PAHs in the ECMSs. North China is an important base for heavy industry and coal, and consumes larger quantities of coal and coke than South China. Furthermore, exhaust gases produced by these industries are emitted into the upper air through tall chimney stacks, allowing transport of pollutants over long distances. The BS and YS are downwind of the Chinese continental outflow during spring and winter. Consequently, there is significant transport of PAHs from the mainland to coastal oceans due to the influence of the East Asian monsoon [*Lang et al.*, 2008]. These PAHs in the upper air can bind to fine particles and are deposited into the ocean due to gravity and precipitation, such as rain, snow, hail [*Chen et al.*, 2016]. Following deposition in the ocean, most PAHs are easily absorbed onto suspended particles, due to their high hydrophobicity and lipid solubility [*Li et al.*, 2006]. This fraction of the total PAHs deposition reaches the bottom sediment through gravity, currents, and biological pump [*Liang*, 2014]. BB is closer to land and smaller than the other subregions, and is predominantly influenced by direct surface runoff and receives limited atmospheric sedimentation. Therefore, the proportion of PAHs from coal combustion in the BB is smaller than in the other subregions (Figure 4). Secondly, PAHs from vehicular sources, which are primarily transported by surface runoff, were mainly distributed in the BB, BS, and SCDMA (Figure 4). Sampling sites in all subregions are near the coast and receive large amounts of river discharge and surface runoff. *Hu et al.* [2011] and *Lin et al.* [2013] have demonstrated that the distribution patterns of organic pollutants (organochlorine pesticides and PAHs) in the SCDMA and ZFCMA are mainly controlled by direct riverine inputs and surface runoff. In addition, coastal currents and shelf sedimentary processes have greater influence on the distribution pattern and fate of organic pollutants in the BS and ECS than in other parts of the study area. *Liu et al.* [2015] reported that PAHs in dry and wet deposition samples in Shanghai, which constituted over 40% of the total PAHs, mainly originated from vehicle exhausts. In addition, PAHs in soil samples collected from Shanghai city also mainly originated from vehicular emissions

21699291, 2017, 6, Downloaded from https://agupubs.onlinelibrary.wiley.com/doi/10.1002/2017JC012890 by Nanjing University, Wiley Online Library on [07/06/2024]. See the Terms and Conditions (https://onlinelibrary.wiley.com/terms-and-conditions) on Wiley Online Library for rules of use; OA articles are governed by the applicable Creative Commons License

[X. T. Wang et al., 2015]. Therefore, the main sources of PAHs in riverine inputs and surface runoff were vehicular emissions. This is related to atmospheric physical processes and physicochemical properties of PAHs; vehicle-exhaust emission sources are closer to the earth surface, resulting in easy absorption of emitted PAHs onto soil particles. Vehicle exhausts also usually have a relatively higher density than normal air, and cannot easily be transported to the upper air and consequently over longer distances. The Bohai economic rim and Yangtze Delta have high car ownership rates, with over 2 million cars registered in 16 cities, including four cities in the Bohai economic rim (Beijing, Tianjin, Shijiazhuang, and Qingdao), four in the Changjiang River Delta (Shanghai, Suzhou, Hangzhou, and Nanjing), and three in the Changjiang River Basin [National Bureau of Statistics of China, 2016]. Therefore, riverine inputs and surface runoff could be the main factors influencing PAH distribution patterns in coastal waters that receive large rivers. The distribution patterns of PAHs in the NYS and SYS are consistent with this hypothesis, as, in the absence of large river discharge into the YS, PAHs mainly originated from atmospheric precipitation [Liu et al., 2012a]. Our calculated results suggested that the influx of atmospheric deposition was closer to the buried flux of PAHs in the YS (Figure 7). PAHs originating from petrogenic sources were mainly distributed near the coast, for example, BB and SCD. In addition to frequent crude oil leaks from the oilfields, the BB is an important shipping center, with harbors such as Tangshan and Tianjin, which release large quantities of oil into the coastal waters. Like the BB, the Changjiang River Estuary is also an important shipping center, with harbors at Shanghai and Yangshan. The cargo throughput of Shanghai is the largest in the world, and the Changjiang (Yangtze) River is one of the most heavily used shipping highways in the world, discharging large amounts of petroleum residues.

3.3. Deposition Flux and Budget of PAHs in the ECMSs

Increasing attention has been paid to PAHs fluxes and budgets, due to the recognized importance of the continental shelf as the major sink of PAHs [Qin et al., 2011; Lin et al., 2013; C. Wang et al., 2016b]; these studies may also contribute significantly toward better understanding of the regional or global carbon cycles. However, the existing studies did not address flux and storage on the continental shelf of the ECMSs, which is adjacent to one of the world's largest PAHs emission source regions [Lang et al., 2008]. Bian et al. [2013] demonstrated that land-derived sediments are transported between subregions of China by of currents, tides, and waves, which consequently also transport sedimentary PAHs. Therefore, we explored the transportation of PAHs in each subregion of the ECMSs and constructed the mass budget of sedimentary PAHs in the ECMSs.

3.3.1. Deposition Flux of PAHs in the ECMSs

Deposition flux of PAHs was calculated using methods described in section 2.2 and the Map Algebra application in ArcGIS 10.2 [C. Wang et al., 2016b]. Data sets of PAHs concentration and sedimentation rate, depicted using the Kriging interpolation method, are shown in Figures 2b and 3a. Detailed information on the distribution pattern of PAHs flux is shown in Figure 5. Compared to the PAHs concentrations, the pattern of PAHs flux is more persuasive, as it has a comprehensive characterization, similar to black carbon, which is not affected by varying inputs and dilution effects [Fang et al., 2015]. PAHs fluxes in the ECMSs ranged from 11.2 to 1308 ng cm^{-2} yr^{-1}, and averaged 101 ± 104 ng cm^{-2} yr^{-1}. The relatively high standard deviation (nearly 103%) indicated that PAHs fluxes show significant spatial differentiation (Figure 5). Among the subregions, the WBS registered the highest PAHs flux, up to 385 ± 255 ng cm^{-2} yr^{-1}, followed by the SCDMA (219 ± 107 ng cm^{-2} yr^{-1}), ZFCMA (166 ± 55 ng cm^{-2} yr^{-1}), open BS (51 ± 18 ng cm^{-2} yr^{-1}), and YS (70.8 ± 30 ng cm^{-2} yr^{-1}). Compared to PAHs concentrations (Figure 2a), the spatial distribution patterns of PAHs flux exhibited obvious differentiation in some subregions such as the SCDMA and YS (Figure 5). PAHs flux near the HRE was relatively high (Figure 5), but PAHs concentrations in the HRE were not very high (Figure 2a). Similarly, PAHs concentrations in the central YS showed relatively high values (Figure 2a), but a high PAHs flux was not observed (Figure 5). Therefore, PAHs flux is an integrated indicator determined by multiple factors, including sedimentation rate and PAHs concentration. On the whole, high values of PAHs flux were mainly distributed in areas of fine-grained sediment such as the BB, HRE, SCDMA, and ZFCMA, demonstrating the importance of shelf mud depositional processes on the fate of PAHs.

We divided the ECMSs into five subregions to calculate the deposition flux, based on the distribution pattern of PAHs accumulation rates. The five subregions were the western BS (WBS), the open BS (OBS), YS, SCDMA, and ZFCMA, with areas of 21,000, 56,000, 197,900, 62,000, and 64,000 km^2, respectively. We

21699291, 2017, 6, Downloaded from https://agupubs.onlinelibrary.wiley.com/doi/10.1002/2017JC012890 by Nanjing University, Wiley Online Library on [07/06/2024]. See the Terms and Conditions (https://onlinelibrary.wiley.com/terms-and-conditions) on Wiley Online Library for rules of use; OA articles are governed by the applicable Creative Commons License

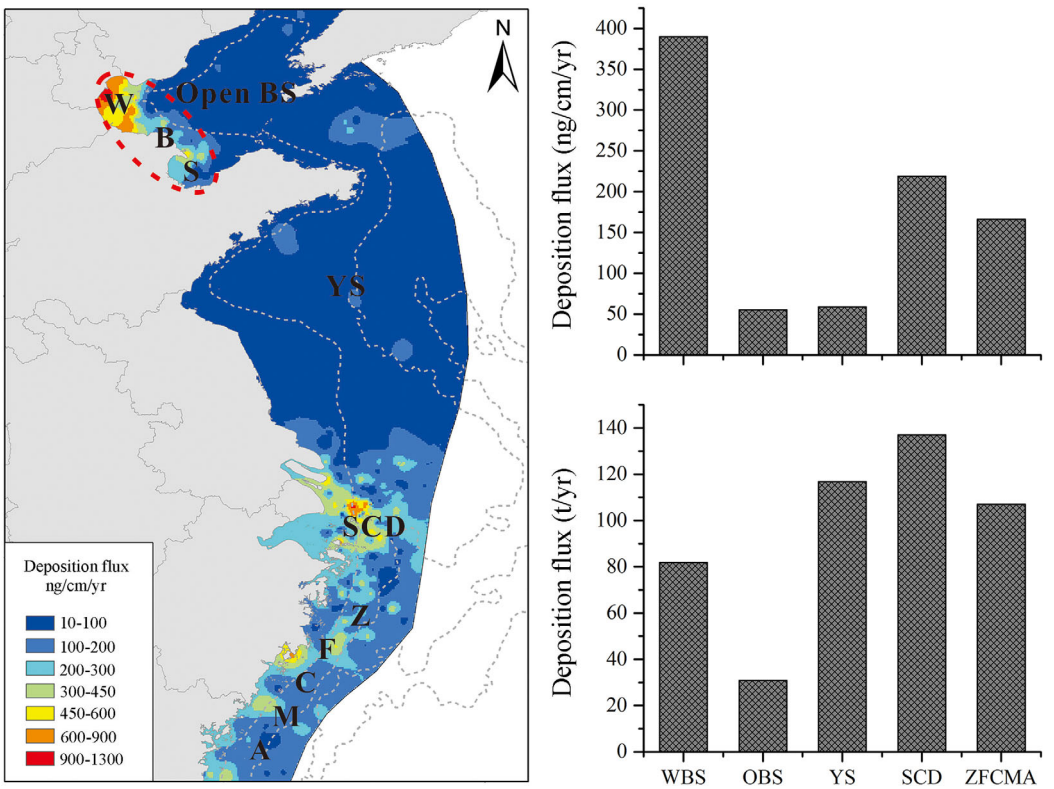

Figure 5. Distribution pattern of PAHs flux in the ECMSs.

calculated the PAHs buried flux in each subregion to be: BB (80.8 ± 53.6 t yr^{-1}); OBS (28.6 ± 10.1 t yr^{-1}); YS (140.6 ± 59.4 t yr^{-1}); SCDMA (137 ± 66.3 t yr^{-1}); and ZFCMA (107 ± 35.2 t yr^{-1}). Our result for the southern BS was significantly different from the value of 36.6 t yr^{-1} calculated by *Qin et al.* [2011]. In our opinion, this phenomenon can be attributed to two effects: (1) the study areas were different, in that our study covered a relatively larger area than that of *Qin et al.* [2011]; (2) data on sedimentation rate was different. The deposition flux of PAHs in the inner shelf regions of ECS and SCDMA calculated by *Lin et al.* [2013] and *C. Wang et al.* [2016b] were consistent with our results.

To assess the importance of PAHs deposition flux in the ECMSs and the biogeochemical processes of PAHs cycles in global coastal zones, we collected worldwide data regarding PAHs fluxes in surface sediments (Figure 6). The continental shelf of the East Asian marginal seas is one of the widest in the world, and receives large amounts of river-derived sediments from large rivers originating in the East Asian Continent. Consequently, large amounts of terrestrial pollutants are discharged into the adjacent marginal seas via riverine runoff and atmospheric deposition. PAHs deposition fluxes have also been studied in the Gulf of Mexico, Mediterranean Sea, and Black Sea (Figure 6). In order to facilitate comparison, the flux per unit area was calculated for all the areas, and is shown in Figure 6 (green column). Comparison of these results suggests that the depositional flux of PAHs in the ECMSs and its subregions is higher than the North Gulf of Mexico, Mediterranean, and SW Black Sea. The highest value was observed in Changjiang Estuary, followed by the inner shelf region of ECS, and the entire region of the ECMSs. With the exception of the East Asian Continent marginal seas, the highest value of PAHs deposition flux occurred in the northern Gulf of Mexico. This study also suggests that the burial efficiency of PAHs in the ECMSs was relatively higher than in the other regions considered. We also used the annual buried flux of PAHs on the regional scale to evaluate the burial capacity of different regions; results are shown in Figure 6 (red column), and indicate that the buried capacity for PAHs in the ECMSs is about 494 t yr^{-1}, which is the highest in the world. Therefore, the ECMSs are an important global sink of PAHs and play a significant role in the global PAHs cycle.

21699291, 2017, 6, Downloaded from https://agupubs.onlinelibrary.wiley.com/doi/10.1002/2017JC012890 by Nanjing University, Wiley Online Library on [07/06/2024]. See the Terms and Conditions (https://onlinelibrary.wiley.com/terms-and-conditions) on Wiley Online Library for rules of use; OA articles are governed by the applicable Creative Commons License

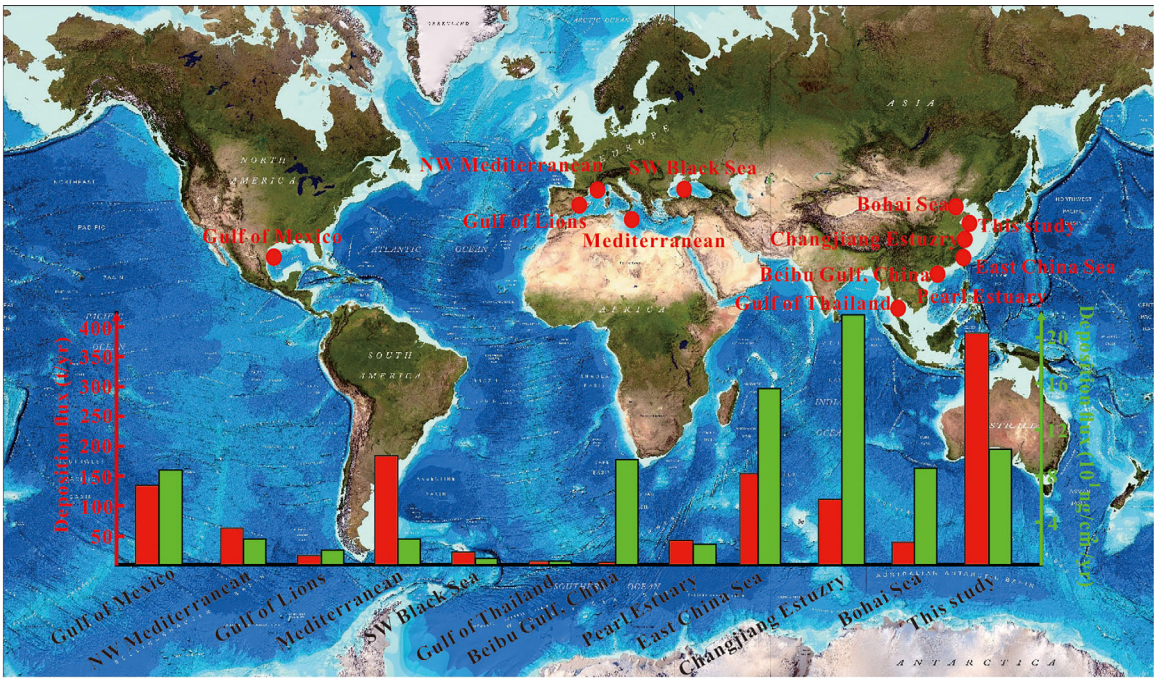

Figure 6. Distribution of reported PAHs flux study in the worldwide (North Gulf of Mexico [*Adhikari et al*., 2015], NW Mediterranean [*Tolosa et al*., 1996], Gulf of Lions [*Bouloubassi et al*., 2012], Mediterranean [*Lipiatou et al*., 1997], SW Black Sea [*Parinos et al*., 2013], Gulf of Thailand [*Hu et al*., 2016b], Beibu Gulf, China [*Li et al*., 2015], Pearl Estuary [*S. J. Chen et al*., 2006], East China Sea [*Lin et al*., 2013], Chiangjiang Estuary [*C. Wang et al*., 2016a,2016b; *J. Wang et al*., 2016], and Bohai Sea [*Qin et al*., 2011]).

3.3.2. PAHs Budget in the ECMSs

Conservation of mass is an important law of nature and is important in scientific research, especially in oceanography. It has been studied in the subregions of the ECMSs. For example, *Deng et al*. [2006] tried to build a mass budget for sediments and TOC in the ECS. *Fang et al*. [2015] successfully constructed the mass budget of black carbon in the BS, and *Gao et al*. [2017] developed a preliminary estimate of the ^{210}Pb budget for the ECS. However, relevant studies in large-scale marginal sea systems are scarce. In this study, we attempted to calculate the PAHs budget in the ECMSs to understand the migration mechanism of PAHs in the ECMSs, using a box model. PAHs inputs into the ECMSs included atmospheric dry and wet deposition ($F_{atmospheric\ \ deposition}$, t yr^{-1}) and riverine input ($F_{riverine\ \ input}$, t yr^{-1}). The outputs consisted of burial to bottom sediment (F_{buried}, t yr^{-1}) and export to outer shelves (F_{output}, t yr^{-1}). The PAHs budget can be described by equation (2).

$$F_{atmospheric\ \ deposition}+F_{riverine\ \ input}=F_{buried}+F_{output} \quad (2)$$

The specific calculation method for the four factors used in equation (2) was derived from *Fang et al*. [2015], and is described in detail in supporting information Text S1. Data on PAHs concentrations in the atmosphere and rivers were collected from published materials [*Wang et al*., 2013; *Chen et al*., 2016; *Qi et al*., 2014; *C. Wang et al*., 2016a] and detailed information is provided in supporting information Tables S1 and S2.

The PAHs budget calculated for the ECMSs is shown in Figure 7. The total PAHs input to the ECMSs was 558.9 t yr^{-1}, with riverine discharge and atmospheric deposition accounting for 159 and 399.9 t yr^{-1}, respectively. The riverine input contributed nearly 28.4% of the total PAHs input into the BS; atmospheric deposition, including wet and dry deposition, was comparable to riverine input and accounted for nearly 71.6% of the total PAHs input. The ECMSs were influenced by the winter and summer East Asian monsoon, which blows through areas of high PAHs emissions in China. *Lin et al*. [2011] demonstrated that origins of PAHs in the surface sediment of the BS and YS were similar to those of the PAHs in $PM_{2.5}$ aerosols from the upwind area, highlighting the significant influence of atmospheric deposition of PAHs in the ECMSs. As for outputs, nearly 88.4% (494 t) of the input PAHs were buried in the bottom sediments, indicating that

21699291, 2017, 6, Downloaded from https://agupubs.onlinelibrary.wiley.com/doi/10.1002/2017JC012890 by Nanjing University, Wiley Online Library on [07/06/2024]. See the Terms and Conditions (https://onlinelibrary.wiley.com/terms-and-conditions) on Wiley Online Library for rules of use; OA articles are governed by the applicable Creative Commons License

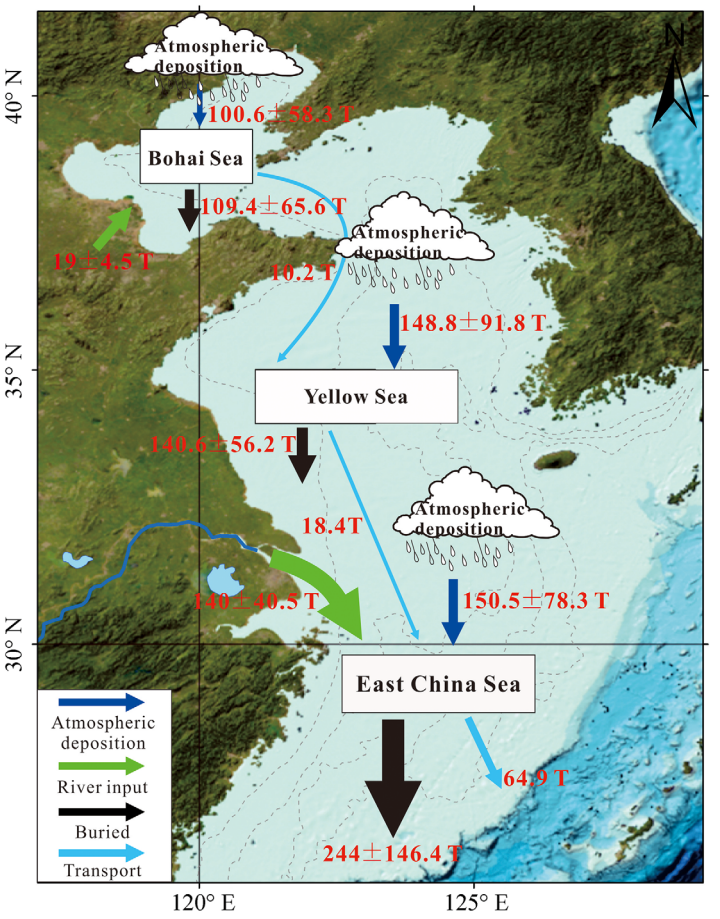

Figure 7. Mass budget of sedimentary PAHs in the ECMSs.

sequestration is the dominant PAHs output pathway, consistent findings for black carbon in the BS, as they are derived from coemitting sources [*Fang et al.*, 2015, 2016]. Therefore, the continental shelf sediments of the ECMSs act as sinks, and play an important role in preserving PAHs originating in China. In addition to the burial effect, transportation of PAHs is also an important factor in the ECMSs. *Fang et al.* [2015] estimated that approximately 9.5% of the annual input of black carbon to the BS was transported to the YS through the Bohai Strait. In this study, we calculated the exchange flux between BS and YS, which accounted for approximately 8.5% of the total influx. Another transmission channel exists between the YS and ECS, and *Tao et al.* [2016] have suggested that the annual export flux of sediment from the YS to ECS was approximately 7.3×10^6 t. This suggests a preliminary estimate of the export flux of PAHs from the YS to ECS of approximately 16.9 t yr^{-1}, which is consistent with our result (18.4 t yr^{-1}). Cross-shelf transportation also plays an important role in PAHs migration, accounting for nearly 11.6% (64.9 t) of the total PAHs input. Previous studies have proved that cross-shelf plumes in the inner shelf region of the ECS provided a major conduit for the transport of sediment across the ECS [*Ren et al.*, 2015; *Gao et al.*, 2017], and facilitated export of large amounts of sedimentary PAHs from the inner shelf to the outer shelf. An export ratio of sediments was defined and calculated as export flux divided by input flux. We calculated an export ratio of 21%, which is very close to the value of 20% proposed by *Gao et al.* [2017]. Thus, the mass budget of PAHs for the ECMSs highlights the fate of PAHs on an extended regional scale and further clarifies the importance of PAHs transportation among subregions of the ECMSs.

4. Conclusions

This study provides an extensive and comprehensive investigation of the PAHs distribution patterns, flux, and budget in the ECMSs, which is situated near areas of high PAHs emissions in China. The major conclusions are:

1. Relatively high PAHs concentrations were mainly observed in areas of fine-grained sediment (i.e., BB, central YS, SCD, and ZFCMA), which also showed high TOC concentrations. This suggests that the spatial distribution patterns of PAHs are largely influenced by regional hydrodynamics and sediment properties. In addition, distribution patterns of PAHs were also influenced by the differing socioeconomic conditions in northern and southern China.
2. The accumulation rate of sedimentary PAHs was estimated to be in the range of 11.2 and 1308 ng cm^{-2} yr^{-1}, with an average value of 101 ± 104 ng cm^{-2} yr^{-1}. The area-integrated PAHs burial flux in the

21699291, 2017, 6, Downloaded from https://agupubs.onlinelibrary.wiley.com/doi/10.1002/2017JC012890 by Nanjing University, Wiley Online Library on [07/06/2024]. See the Terms and Conditions (https://onlinelibrary.wiley.com/terms-and-conditions) on Wiley Online Library for rules of use; OA articles are governed by the applicable Creative Commons License

ECMSs was 494 t yr^{-1}, accounting for 88.4% of the input PAHs, with the WBS, OBS, YS, SCD, and ZFCMA subregions accounting for approximately 80.8, 28.6, 140.6, 137, and 107 t yr^{-1}, respectively.

3. The PAHs budget in the ECMSs was calculated. The total PAHs flux input into the ECMSs is nearly 558.9 t yr^{-1}, with riverine discharge and atmospheric deposition accounting for 159 and 399.9 t yr^{-1}, respectively. In addition, the cross-shelf plume provides a major conduit for the transport of PAHs from the inner to the outer shelf of the ECS, which constituted about 8.3% of the PAHs flux input into the ECMSs.

Acknowledgments
The study was supported by the National Basic Research Program of China (grant 2013CB956503) and the National Science Foundation of China (grant 41471431). Two anonymous reviewers provided thoughtful and high valuable comments, suggestions, and advises which greatly improved the quality of this manuscript. The data for this study are available from the corresponding author via email: zouxq@nju.edu.cn, and all numerical data are also showed in supporting information.

References

Adhikari, P. L., K. Maiti, and E. B. Overton (2015), Vertical fluxes of polycyclic aromatic hydrocarbons in the Northern Gulf of Mexico, *Mar. Chem.*, *168*(3), 60–68.

Ali, U., J. H. Syed, L. Junwen, L. Sánchez-García, R. N. Malik, M. J. Chaudhry, M. Arshad, J. Li, G. Zhang, and K. C. Jones (2014), Assessing the relationship and influence of black carbon on distribution status of organochlorines in the coastal sediments from Pakistan, *Environ. Pollut.*, *190*(4), 82–90.

Bai, F. C., and Z. K. Sun (2007), Research on the desulfurization technology of coal-fired power plants in Bohai Gulf [in Chinese], *Electric Power Environ. Protect.*, *235*), 24–26.

Bian, C., W. Jiang, and R. J. Greatbatch (2013), An exploratory model study of sediment transport sources and deposits in the Bohai Sea, Yellow sea, and East China Sea, *J. Geophys. Res. Oceans*, *118*, 5908–5923, doi:10.1002/2013JC009116.

Bianchi, T. S. (2011), The role of terrestrially derived organic carbon in the coastal ocean: A changing paradigm and the priming effect, *Proc. Natl. Acad. Sci. U. S. A.*, *108*(49), 19,473–19,481.

Bouloubassi, I., V. Roussiez, M. Azzoug, and A. Lorre (2012), Sources, dispersal pathways and mass budget of sedimentary polycyclic aromatic hydrocarbons (PAHs) in the NW Mediterranean margin, Gulf of Lions, *Mar. Chem.*, *142–144*(11), 18–28.

Chen, S. J., X. J. Luo, B. X. Mai, G. Y. Sheng, J. M. Fu, and E. Y. Zeng (2006), Distribution and mass inventories of polycyclic aromatic hydrocarbons and organochlorine pesticides in sediments of the Pearl River Estuary and the northern South China Sea, *Environ. Sci. Technol.*, *40*(3), 709–714.

Chen, Y., D. Hu, and Y. Weng (2006), The research on the concentration size distribution and source of PAHs in particulate in Ningbo [in Chinese], *Environ. Monit. China*, *22*(2), 59–61.

Chen, Y., T. Lin, J. Tang, Z. Xie, C. Tian, J. Li, and G. Zhang (2016), Exchange of polycyclic aromatic hydrocarbons across the air-water interface in the Bohai and Yellow Seas, *Atmos. Environ.*, *141*, 153–160.

Deng, B., J. Zhang, and Y. Wu (2006), Recent sediment accumulation and carbon burial in the East China Sea, *Global Biogeochem. Cycles*, *20*, GB3014, doi:10.1029/2005GB002559.

Dong, L. X., W. B. Guan, Q. Chen, X. H. Li, X. H. Liu, and X. M. Zeng (2011), Sediment transport in the Yellow Sea and East China Sea, *Estuarine Coastal Shelf Sci.*, *93*(3), 248–258.

Fang, Y., Y. Chen, C. Tian, T. Lin, L. Hu, G. Huang, J. H. Tang, J. Li, and G. Zhang (2015), Flux and budget of BC in the continental shelf seas adjacent to Chinese high BC emission source regions, *Global Biogeochem. Cycles*, *29*, 957–972, doi:10.1002/2014GB004985.

Fang, Y., Y. Chen, C. Tian, T. Lin, L. Hu, J. Li, and G. Zhang (2016), Application of PMF receptor model merging with PAHs signatures for source apportionment of black carbon in the continental shelf surface sediments of the Bohai and Yellow Seas, China, *J. Geophys. Res. Oceans*, *121*, 1346–1359, doi:10.1002/2015JC011214.

Gao, J. H., et al. (2017), Variations in the transport, distribution and budget of 210Pb in sediment over the estuarine and inner shelf areas of the East China Sea due to Changjiang catchment changes, *J. Geophys. Res. Earth Surf.*, *122*, 235–247, doi:10.1002/2016JF004130.

Gao, X., F. Zhou, and C. T. A. Chen (2014), Pollution status of the Bohai Sea: An overview of the environmental quality assessment related trace metals, *Environ. Int.*, *62*, 12–30.

González-Gaya, B., M. C. Fernández-Pinos, L. Morales, L. Méjanelle, E. Abad, B. Piña, C. M. Duarte, B. Jiménez, and J. Dachs (2016), High atmosphere-ocean exchange of semivolatile aromatic hydrocarbons, *Nat. Geosci.*, *9*(6), 438–442.

Guo, Z., T. Lin, G. Zhang, Z. Yang, and M. Fang (2006), High-resolution depositional records of polycyclic aromatic hydrocarbons in the central continental shelf mud of the East China Sea, *Environ. Sci. Technol.*, *40*(17), 5304–5311.

Han, Y. M., et al. (2015), Elemental carbon and polycyclic aromatic compounds in a 150-year sediment core from Lake Qinghai, Tibetan Plateau, China: Influence of regional and local sources and transport pathways, *Environ. Sci. Technol.*, *49*(7), 4176–4183.

Hu, B., G. Li, J. Li, M. Yang, L. B. Wang, and R. Y. Bu (2011), Spatial variability of the 210 Pb sedimentation rates in the Bohai and Huanghai Seas and its influencing factors [in Chinese with English abstract], *Acta Oceanol. Sin.*, *33*(6), 125–133.

Hu, L., X. Shi, Z. Yu, T. Lin, H. Wang, D. Ma, Z. Guo, and Z. Yang (2012), Distribution of sedimentary organic matter in estuarine–inner shelf regions of the East China Sea: Implications for hydrodynamic forces and anthropogenic impact, *Mar. Chem.*, *142*, 29–40.

Hu, L., X. Shi, Z. Guo, H. Wang, and Z. Yang (2013), Sources, dispersal and preservation of sedimentary organic matter in the Yellow Sea: The importance of depositional hydrodynamic forcing, *Mar. Geol.*, *335*, 52–63.

Hu, L., X. Shi, T. Lin, Z. Guo, D. Ma, and Z. Yang (2014), Perylene in surface sediments from the estuarine-inner shelf of the East China Sea: A potential indicator to assess the sediment footprint of large river influence, *Cont. Shelf Res.*, *90*, 142–150.

Hu, L., X. Shi, Y. Bai, S. Qiao, L. Li, Y. Yu, G. Yang, D. Ma, and Z. Guo (2016a), Recent organic carbon sequestration in the shelf sediments of the Bohai Sea and Yellow Sea, *China, J. Mar. Syst.*, *155*, 50–58.

Hu, L., X. Shi, S. Qiao, T. Lin, Y. Li, Y. Bai, and B. Wu (2016b), Sources and mass inventory of sedimentary polycyclic aromatic hydrocarbons in the Gulf of Thailand: Implications for pathways and energy structure in SE Asia, *Sci. Total Environ.*, *575*, 982–995.

Huang, D., J. Su, and J. O. Backhaus (1999), Modelling the seasonal thermal stratification and baroclinic circulation in the Bohai Sea, *Cont. Shelf Res.*, *19*(11), 1485–1505.

Huang, L., and S. A. Batterman (2014), Multimedia model for polycyclic aromatic hydrocarbons (PAHs) and nitro-pahs in Lake Michigan, *Environ. Sci. Technol.*, *48*(23), 13,817–13,825.

Khairy, M. A., M. P. Weinstein, and R. Lohmann (2014), Trophodynamic behavior of hydrophobic organic contaminants in the aquatic food web of a tidal river, *Environ. Sci. Technol.*, *48*(21), 12,533–12,542.

Kim, G. B., K. A. Maruya, R. F. Lee, J. H. Lee, C. H. Koh, and S. Tanabe (1999), Distribution and sources of polycyclic aromatic hydrocarbons in sediments from Kyeonggi Bay, Korea, *Mar. Pollut. Bull.*, *38*(1), 7–15.

Lang, C., S. Tao, W. Liu, Y. Zhang, and S. Simonich (2008), Atmospheric transport and outflow of polycyclic aromatic hydrocarbons from China, *Environ. Sci. Technol.*, *42*(14), 5196–5201.

21699291, 2017, 6, Downloaded from https://agupubs.onlinelibrary.wiley.com/doi/10.1002/2017JC012890 by Nanjing University, Wiley Online Library on [07/06/2024]. See the Terms and Conditions (https://onlinelibrary.wiley.com/terms-and-conditions) on Wiley Online Library for rules of use; OA articles are governed by the applicable Creative Commons License

Leithold, E. L., N. E. Blair, and K. W. Wegmann (2016), Source-to-sink sedimentary systems and global carbon burial: A river runs through it, *Earth Sci. Rev.*, *153*, 30–42.
Li, G., X. Xia, Z. Yang, R. Wang, and N. Voulvoulis (2006), Distribution and sources of polycyclic aromatic hydrocarbons in the middle and lower reaches of the yellow river, China, *Environ. Pollut.*, *144*(3), 985–993.
Li, L., X. J. Wang, J. H. Liu, and X. F. Shi (2017), Dissolved trace metal (Cu, Cd, Co, Ni, and Ag) distribution and Cu speciation in the southern Yellow Sea and Bohai Sea, China, *J. Geophys. Res. Oceans*, *122*, 1190–1205, doi:10.1002/2016JC012500.
Li, P., R. Xue, Y. Wang, R. Zhang, and G. Zhang (2015), Influence of anthropogenic activities on PAHs in sediments in a significant gulf of low-latitude developing regions, the Beibu Gulf, South China Sea: Distribution, sources, inventory and probability risk, *Mar. Pollut. Bull.*, *90*(1–2), 218–226.
Li, W. H., Y. Z. Tian, G. L. Shi, C. S. Guo, X. Li, and Y. C. Feng (2012), Concentrations and sources of PAHs in surface sediments of the Fenhe reservoir and watershed, China, *Ecotoxicol. Environ. Safety*, *75*(1), 198–206.
Li, Y., T. Lin, L. Hu, J. Feng, and Z. Guo (2016), Time trends of polybrominated diphenyl ethers in east China seas: Response to the booming of PBDE pollution industry in China, *Environ. Int.*, *92–93*, 507–514.
Liang, J. H. (2014), The study on distribution, biological pump output and time series of PAHs in the South China Sea, PhD dissertation, pp. 12–14, Xiamen Univ., Xiamen, China.
Lima, A. L., T. I. Eglinton, and C. M. Reddy (2003), High-resolution record of pyrogenic polycyclic aromatic hydrocarbon deposition during the 20th century, *Environ. Sci. Technol.*, *37*(1), 53–61.
Lin, T., L. Hu, Z. Guo, Y. Qin, Z. Yang, G. Zhang, and M. Zheng (2011), Sources of polycyclic aromatic hydrocarbons to sediments of the Bohai and Yellow Seas in East Asia, *J. Geophys. Res. Atmos.*, *116*, D23305, doi:10.1029/2011JD015722.
Lin, T., L. Hu, Z. Guo, G. Zhang, and Z. Yang (2013), Deposition fluxes and fate of polycyclic aromatic hydrocarbons in the Yangtze River estuarine-inner shelf in the East China Sea, *Global Biogeochem. Cycles*, *27*, 77–87, doi:10.1029/2012GB004317.
Lin, X., L. Hou, M. Liu, X. Li, Y. Zheng, G. Yin, J. Gao, and X. Jiang (2016). Nitrogen mineralization and immobilization in sediments of the East China Sea: Spatiotemporal variations and environmental implications, *J. Geophys. Res. Biogeosci.*, *121*, 2842–2855, doi:10.1002/2016JG003499.
Lipiatou, E., et al. (1997), Mass budget and dynamics of polycyclic aromatic hydrocarbons in the Mediterranean Sea, *Deep Sea Res., Part II*, *44*(3–4), 881–905.
Liu, G. R., X. Peng, R. K. Wang, Y. Z. Tian, G. L. Shi, J. H. Wu, P. Zhang, L. D. Zhou, and Y. C. Feng (2015), A new receptor model-incremental lifetime cancer risk method to quantify the carcinogenic risks associated with sources of particle-bound polycyclic aromatic hydrocarbons from Chengdu in China, *J. Hazardous Mater.*, *283*, 462–468.
Liu, J. P., K. H. Xu, A. E. A. Li, J. D. Milliman, D. M. Velozzi, S. B. Xiao, and Z. S. Yang (2007), Flux and fate of Yangtze River sediment delivered to the East China Sea, *Geomorphology*, *85*(3), 208–224.
Liu, L. Y., J. Z. Wang, G. L. Wei, Y. F. Guan, C. S. Wong, and E. Y. Zeng (2012a), Sediment records of polycyclic aromatic hydrocarbons (PAHs) in the continental shelf of China: Implications for evolving anthropogenic impacts, *Environ. Sci. Technol.*, *46*(12), 6497–6504.
Liu, L. Y., J. Z. Wang, G. L. Wei, Y. F. Guan, and E. Y. Zeng (2012b), Polycyclic aromatic hydrocarbons (PAHs) in continental shelf sediment of China: Implications for anthropogenic influences on coastal marine environment, *Environ. Pollut.*, *167*(12), 155–162.
Liu, L. Y., G. L. Wei, J. Z. Wang, Y. F. Guan, C. S. Wong, F. C. Wu, and E. Y. Zeng (2013), Anthropogenic activities have contributed moderately to increased inputs of organic materials in marginal seas off China, *Environ. Sci. Technol.*, *47*(20), 11,414–11,422.
Liu, W. X., J. L. Chen, X. M. Lin, and S. Tao (2006), Distribution and characteristics of organic micropollutants in surface sediments from Bohai Sea, *Environ. Pollut.*, *140*(1), 4–8.
Liu, Y. K., Q. Wang, M. Liu, M. Lu, S. Liu, B. Yang, Z. L. Wu, and Y. K. Qin (2015), Concentration characteristics and potential sources of polycyclic aromatic hydrocarbons in atmospheric deposition in Shanghai [in Chinese with English abstract], *Chin. Environ. Sci.*, *35*(9), 2605–2614.
Lohmann, R., R. Gioia, K. C. Jones, L. Nizzetto, C. Temme, Z. Xie, D. Schulz-Bull, I. Hand, E. Morgan, and L. Jantunen (2009), Organochlorine pesticides and PAHs in the surface water and atmosphere of the north Atlantic and Arctic Ocean, *Environ. Sci. Technol.*, *43*(15), 5633–5639.
Mulder, M. D., A. Heil, P. Kukučka, J. Klánová, J. Kuta, R. Prokeš, F. Sprovieri, and G. Lammel (2014), Air–sea exchange and gas–particle partitioning of polycyclic aromatic hydrocarbons in the Mediterranean, *Atmos. Chem. Phys.*, *14*(17), 8905–8915.
Mwangi, J. K., W. J. Lee, L. C. Wang, P. J. Sung, L. S. Fang, Y. Y. Lee, and G. P. Chang-Chien (2016), Persistent organic pollutants in the Antarctic coastal environment and their bioaccumulation in penguins, *Environ. Pollut.*, *216*, 924–934.
National Bureau of Statistics of China (2016), *China Economic Yearbook in 2016*, Beijing.
Parinos, C., A. Gogou, I. Bouloubassi, S. Stavrakakis, E. Plakidi, and I. Hatzianestis (2013), Sources and downward fluxes of polycyclic aromatic hydrocarbons in the open southwestern Black Sea, *Organic Geochem.*, *57*(4), 65–75.
Park, J. H., A. H. Goldstein, J. Timkovsky, S. Fares, R. Weber, J. Karlik, and R. Holzinger (2013), Active atmosphere-ecosystem exchange of the vast majority of detected volatile organic compounds, *Science*, *341*(6146), 643–647.
Qi, W., et al. (2014), Organic micropollutants in the Yangtze River: seasonal occurrence and annual loads, *Sci. Total Environ.*, *472*, 789–799.
Qin, Y., B. Zheng, K. Lei, T. Lin, L. Hu, and Z. Guo (2011), Distribution and mass inventory of polycyclic aromatic hydrocarbons in the sediments of the south Bohai Sea, China, *Mar. Pollut. Bull.*, *62*(2), 371–376.
Qin, Y. S., Y. Y. Zhao, L. R. Chen, and S. L. Zhao (1990), *Geology of Bohai Sea [in Chinese]*, pp. 1–354, China Ocean Press, Beijing.
Ren, J. L., J. L. Xuan, Z. W. Wang, D. Huang, and J. Zhang (2015), Cross-shelf transport of terrestrial Al enhanced by the transition of northeasterly to southwesterly monsoon wind over the East China Sea, *J. Geophys. Res. Oceans*, *120*, 5054–5073, doi:10.1002/2014JC010655.
Shi, G. L., X. Li, Y. C. Feng, Y. Q. Wang, J. H. Wu, J. Li, and T. Zhu (2009), Combined source apportionment, using positive matrix factorization–chemical mass balance and principal component analysis/multiple linear regression–chemical mass balance models, *Atmos. Environ.*, *43*(18), 2929–2937.
Stout, S. A., and T. P. Graan (2010), Quantitative source apportionment of PAHs in sediments of Little Menomonee River, Wisconsin: Weathered creosote versus urban background, *Environ. Sci. Technol.*, *44*(8), 2932–2939.
Sverdrup, L. E., T. Nielsen, and P. H. Krogh (2002), Soil ecotoxicity of polycyclic aromatic hydrocarbons in relation to soil sorption, lipophilicity, and water solubility, *Environ. Sci. Technol.*, *36*(11), 2429–2435.
Tao, S., T. I. Eglinton, D. B. Montluçon, C. Mcintyre, and M. Zhao (2016), Diverse origins and pre-depositional histories of organic matter in contemporary Chinese marginal sea sediments, *Geochim. Cosmochim. Acta*, *191*, 70–88.
Tolosa, I., J. M. Bayona, and I. Albaiges (1996), Aliphatic and polycyclic aromatic hydrocarbons and sulfur/oxygen derivatives in northwestern Mediterranean sediments: Spatial and temporal variability, fluxes, and budgets, *Environ. Sci. Technol.*, *30*(8), 2495–2503.
Wang, C., S. Wu, S. Zhou, H. Wang, B. Li, H. Chen, Y. Yu, and Y. Shi (2015), Polycyclic aromatic hydrocarbons in soils from urban to rural areas in Nanjing: Concentration, source, spatial distribution, and potential human health risk, *Sci. Total Environ.*, *527*, 375–383.

21699291, 2017, 6, Downloaded from https://agupubs.onlinelibrary.wiley.com/doi/10.1002/2017JC012890 by Nanjing University, Wiley Online Library on [07/06/2024]. See the Terms and Conditions (https://onlinelibrary.wiley.com/terms-and-conditions) on Wiley Online Library for rules of use; OA articles are governed by the applicable Creative Commons License

Wang, C., X. Zou, Y. Zhao, B. Li, Q. Song, Y. Li, and W. Yu (2016a), Distribution, sources, and ecological risk assessment of polycyclic aromatic hydrocarbons in the water and suspended sediments from the middle and lower reaches of the Yangtze River, China, *Environ. Sci. Pollut. Res. Int.*, *23*(17), 1–13.

Wang, C., X. Zou, J. Gao, Y. Zhao, W. Yu, Y. Li, and Q. Song (2016b), Pollution status of polycyclic aromatic hydrocarbons in surface sediments from the Yangtze River estuary and its adjacent coastal zone, *Chemosphere*, *162*, 80–90.

Wang, F., T. Lin, Y. Li, T. Ji, C. Ma, and Z. Guo (2014), Sources of polycyclic aromatic hydrocarbons in PM2.5 over the East China Sea, a downwind domain of East Asian continental outflow, *Atmos. Environ.*, *92*(9), 484–492.

Wang, J. Z., Y. F. Guan, H. G. Ni, X. L. Luo, and E. Y. Zeng (2007), Polycyclic aromatic hydrocarbons in riverine runoff of the Pearl River Delta (China): Concentrations, fluxes, and fate, *Environ. Sci. Technol.*, *41*(16), 5614–5619.

Wang, X. T., L. Chen, X. K. Wang, B. L. Lei, Y. F. Sun, J. Zhou, and M.-H. Wu (2015), Occurrence, sources and health risk assessment of polycyclic aromatic hydrocarbons in urban (Pudong) and suburban soils from shanghai in China, *Chemosphere*, *119*, 1224–1232.

Wang, Z., P. Ren, Y. Sun, X. Ma, X. Liu, G. Na, and Z. Yao (2013), Gas/particle partitioning of polycyclic aromatic hydrocarbons in coastal atmosphere of the north Yellow Sea, China, *Environ. Sci. Pollut. Res.*, *20*(8), 5753–5763.

Xia, C., F. Qiao, Y. Yang, J. Ma, and Y. Yuan (2006), Three-dimensional structure of the summertime circulation in the Yellow Sea from a wave-tide-circulation coupled model, *J. Geophys. Res.*, *111*, C11S03, doi:10.1029/2005JC003218.

Xing, J., J. Song, H. Yuan, X. Li, N. Li, L. Duan, X. Kang, and Q. Wang (2017), Fluxes, seasonal patterns and sources of various nutrient species (nitrogen, phosphorus and silicon) in atmospheric wet deposition and their ecological effects on Jiaozhou Bay, North China, *Sci. Total Environ.*, *576*, 617–627.

Xing, L., M. Zhao, W. Gao, F. Wang, H. Zhang, L. Li, J. Liu, and Y. Liu (2014), Multiple proxy estimates of source and spatial variation in organic matter in surface sediments from the southern Yellow Sea, *Organic Geochem.*, *76*, 72–81.

Xu, K., A. Li, J. P. Liu, J. D. Milliman, Z. Yang, C. S. Liu, S. J. Kao, S. M. Wan, and F. Xu (2012), Provenance, structure, and formation of the mud wedge along inner continental shelf of the East China Sea: A synthesis of the Yangtze dispersal system, *Mar. Geol.*, *291*, 176–191.

Yang, Z. S., and J. P. Liu (2007), A unique Yellow River-derived distal subaqueous delta in the Yellow Sea, *Mar. Geol.*, *240*(1), 169–176.

Yim, U. H., S. H. Hong, S. Y. Ha, G. M. Han, J. G. An, N. S. Kim, D.-i. Lim, H.-W. Choi, and W. J. Shim (2014), Source- and region-specific distribution of polycyclic aromatic hydrocarbons in sediments from Jinhae Bay, Korea, *Sci. Total Environ.*, *470–471*(2), 1485–1493.

Yuan, D., and Y. Hsueh (2010), Dynamics of the cross-shelf circulation in the Yellow and East China Seas in winter, *Deep Sea Res., Part II*, *57*(19), 1745–1761.

Yuan, G. L., J. X. Qin, J. Li, X. X. Lang, and G. H. Wang (2014), Persistent organic pollutants in soil near the Changwengluozha glacier of the Central Tibetan Plateau, China: Their sorption to clays and implication, *Sci. Total Environ.*, *472*, 309–315.

Zeng, X., R. He, Z. Xue, H. Wang, Y. Wang, Z. Yao, W. Guan, and J. Warrillow (2015), River-derived sediment suspension and transport in the Bohai, Yellow, and East China Seas: A preliminary modeling study, *Cont. Shelf Res.*, *111*, 112–125.

Zeng, L. X., et al. (2012), Distribution of short chain chlorinated paraffins in marine sediments of the East China Sea: Influencing factors, transport and implications, *Environ. sci. Technol.*, *46*(18), 9898–9906.

Zhang, A. Y., J. Zhang, J. Hu, R. F. Zhang, and G. S. Zhang (2015), Silicon isotopic chemistry in the Changjiang Estuary and coastal regions: Impacts of physical and biogeochemical processes on the transport of riverine dissolved silica, *J. Geophys. Res. Oceans*, *120*, 6943–6957, doi:10.1002/2015JC011050.

Zhang, K., and H. W. Gao (2007), The characteristics of Asian-dust storms during 2000–2002: From the source to the sea, *Atmos. Environ.*, *41*(39), 9136–9145.

Zhang, Y., and S. Tao (2009), Global atmospheric emission inventory of polycyclic aromatic hydrocarbons (PAHs) for 2004, *Atmos. Environ.*, *43*(4), 812–819.

Zhang, Y., C. S. Guo, J. Xu, Y. Z. Tian, G. L. Shi, and Y. C. Feng (2012), Potential source contributions and risk assessment of PAHs in sediments from Taihu Lake, China: Comparison of three receptor models, *Water Res.*, *46*(9), 3065–3073.

Zhao, Y., X. Zou, J. Gao, X. Xu, C. Wang, D. Tang, T. Wang, and X. Wu (2015), Quantifying the anthropogenic and climatic contributions to changes in water discharge and sediment load into the sea: a case study of the Yangtze River, China, *Sci. Total Environ.*, *536*, 803–812.

Zhao, Y., X. Zou, J. Gao, and C. Wang (2017), Recent sedimentary record of storms and floods within the estuarine-inner shelf region of the East China Sea, *The Holocene*, *27*(3), 439–449.

Zhong, G., J. Tang, Z. Xie, A. Möller, Z. Zhao, R. Sturm, (2014). Selected current-use and historic-use pesticides in air and seawater of the Bohai and Yellow seas, China, *J. Geophys. Res. Atmos.*, *119*, 1073–1086, doi:10.1002/2013JD020951.

Zhu, Y. (2014), Characteristics and sources of particulate polycyclic aromatic hydrocarbon (PAHs) in the Yellow River Delta [in Chinese], Master's thesis, pp. 22–23, Shandong Univ., Shandong, China.

21699291, 2017, 6, Downloaded from https://agupubs.onlinelibrary.wiley.com/doi/10.1002/2017JC012890 by Nanjing University, Wiley Online Library on [07/06/2024]. See the Terms and Conditions (https://onlinelibrary.wiley.com/terms-and-conditions) on Wiley Online Library for rules of use; OA articles are governed by the applicable Creative Commons License